NASA TECHNICAL MEMORANDUM NASA TM-75816

THE AERODYNAMICS OF SMALL REYNOLDS NUMBERS

F.W. Schmitz

Translation of "Zur Aerodynamik der kleinen Reynolds-Zahlen,"Jahrbuch 1953 der Wissenschaftlichen Gesellschaft für Luftfahrt E.V. mit den Vorträgen der WGL-Tagung in Göttingen, May 26-29, 1953, Braunschweig, West Germany, Friedr. Vieweg & Sohn, 1954, pp. 149-166

NATIONAL AERONAUTICS AND SPACE ADMINISTRATION
WASHINGTON, D.C. 20546 JUNE 1980

STANDARD TITLE PAGE

1. Report No. NASA TM-75816	2 Government Accession No.	3 Recipient's Catalog No.
4. Title and Subtitle The aerodynamics of small Reynolds numbers		5. Report Date June 1980 6. Performing Organization Code
7. Author(s) F. W. Schmitz		8. Performing Organization Report No. 10 Work Unit No.
9. Performing Organization Name and Address Leo Kanner Associates Redwood City CA 94063		11. Contract or Grant No. NASW-3199 13. Type of Report and Period Covered Translation
12. Sponsoring Agency Name and Address National Aeronautics and Space Administration, Washington DC 20546		14. Sponsoring Agency Code

15. Supplementary Notes

Translation of "Zur Aerodynamik der kleinen Reynolds-Zahlen," Jahrbuch 1953 der Wissenschaftlichen Gesellschaft für Luftfahrt E.V. mit den Vorträgen der WGL-Tagung in Göttingen, May 26-29, 1953, Braunschweig, West Germany, Friedr. Vieweg & Sohn, 1954, pp. 149-166.

16. Abstract

Aerodynamic characteristics of wing models--gliders and bird wings--are discussed. Experimental results are given, and an artificial bird wing is described.

17. Key Words (Selected by Author(s))	18. Distribution Statement		
	Unclassified - Unlimited		
19. Security Classif. (of this report) Unclassified	20. Security Classif. (of this page) Unclassified	21. No. of Pages 47	22. Price

NASA HQ

THE AERODYNAMICS OF SMALL REYNOLDS NUMBERS

F.W. Schmitz

/149*

1. Generating Supporting Data for Work on the "Ludwig-Prandtl-Prize"

The airfoil measurements discussed in the following replenish the wind tunnel measurements (from 1937 to 1945) communicated in Report No. 130 of the Lilienthal-Society, viz., presented explicitly in the book of the author [18], in the range of Reynolds numbers <200,000. The surprising results cleared up the behavior of the airfoil in the critical transition from the laminar to the turbulent boundary layer, which plays a more complex role in model or bird wings than in large airplanes.

These results should give schools especially a basis for a connection between flight physics and its practical application in airplane model construction. For this purpose it is the task of the "Committee for Aerodynamics at Low Velocities," which was formed as part of the Scientific Society for Aeronautics in 1953, to generate further data for the 1937 announced "Ludwig-Prandtl Prize for the promotion of flight physics in connection with airplane model construction" by the Lilienthal-Society for Aeronautical Research, and renewed 1953 by the WGL, respectively. Essentially, the results of this work for the "Ludwig-Prandtl Prize" are to serve the interested teachers and students as basis for the solution of experimental and theoretical tasks in scientific teams of advanced level schools and technical colleges, to generate a vocational stimulus for aeronautical studies. In accordance with this aim an attempt will be made below to describe the problems in a manner for general understanding.

2. Re--Number Ranges

The Reynolds-number $Re = \frac{vt}{\nu}$ denotes the physical dimensional relationship of the flow around a body (velocity v in cm/s, profile

*Numbers in the margin indicate pagination in the foreign text.

depth t in cm, kinematic viscosity of air v = 0.143 cm e/s at 13°C and 760 torr). The first table of numbers gives an overview over the Re-number range from commercial airplane to butterfly.

Table 1.

Commercial airplanes	Re ≈ 3.10^7
Sport airplanes	10^7
Gliders at v_{max}	3.10^6
Gliders at v_{min}	6.10^5
Training gliders	10^6
Captive aircraft models	Re ≈ 120,000...320,000
Large motorized airplane models	60,000...160,000
Medium size motorized and large glider models	30,000...100,000
Small airplane models	15,000... 60,000
Hangar airplane models	5,000... 30,000
Albatros sailing	Re ≈ 200,000
Silver gull sailing	100,000
Wall sailor gliding	42,000
Butterfly gliding	3,000... 7,000

With the exception of the largest ocean flying Albatros (v = 16 m/s) and the fast (v = 20 to 50 m/s) flying captive aircraft, the flight of both models and birds happens to be below the very low Re-number limit of about 150,000. This is a region in which the flow around the airfoil, as well as its force, have the unpleasant quality of changing spasmodically. Beyond this range in the standard flight region up to the proximity of sonic speed no spasmodic but only a small, continuous and rational change may be observed. The well-known Göttinger profiles [1]), measured at Re ≈ 420,000, are adequate for the region of gliders and small private airplanes, each with a polar diagram, but not for the region of model and bird flight, as the following series of measurements covering the small region of Re ≈ 14,000 to 180,000 per profiles covering 2 to 8 polars, show. Each airfoil must overcome a critical flow condition within

this region, since the subcritical laminar detached boundary layer of the upper airfoil at low velocities becomes turbulent at a critical Re-number and becomes attached; the lift then increases spasmodically, the drag decreases correspondingly and model and bird become airworthy.

The smaller the flight model the more desirable is the turbulent, hypercritical condition at a smaller Re-number. This can be achieved by a suitable choice of airfoil or by means of artificial turbulence, as shown by nature in the flight of birds and insects.

In contrast to the above, pains are taken to maintain the /150
laminar condition of the boundary layer of large airplanes, with flight ranges of 10-100 times the Re-number, as long as possible because of its low friction resonance. This is done by using highest surface polish and by "laminar profiles," since turbulence is achieved there anyway. The airplane model flies better with a "turbulent profile," which is similar to the profile of a bird wing. Moreover, the bird feathers have great relative roughness; the dragonfly wings have even transverse folds and a sharp-toothed front edge. The large airplane wing is prone to crash even with a small amount of ice buildup at the leading edge.

3. Justification of Special Test Methods

The Re-number signifies the ratio of the work of acceleration to the friction of a body in a flowing medium, or the ratio of the mean movement of inertia to the viscosity of the flowing medium. For a large Re-number inertia forces govern the flow condition; for a low Re-number the viscosity forces do it. The laminar condition of flow at low Re-number is, therefore, to be interpreted in such a manner that with adequate viscosity small perturbations are dampened, a certain wall roughness is smoothened and the laminar surface friction is therefore smaller than the turbulent one for the same Re-number. This is well known and the points of instability

may be calculated by means of the new boundary layer theory of Tollinsen and Schlichting [3].

To describe and measure laminar flow processes on flight bodies in wind tunnels correctly, the air flow must be made largely turbulence-free. For this purpose, five means are available:

1. Installation of 2 or 3 fine wire mesh sieves in the jet prechamber with a total $c_{wR} \leq 2$, which are mounted behind the honeycomb at 30 cm distances with the c_{wR} decreasing towards the jet.
2. Installation of a long region of stabilized flow between wire mesh sieves and the jet, as well as the most important measure:
3. Installation of a slender jet with a contraction ratio of at least 5:1 (maximum of 20:1) since convergent flow, or pressure drop, constitute reductions of turbulence.
4. A collecting cone with a well rounded inlet, small diffuser expansion angle and not too small outer and inner diameters, to prevent low frequency vibrations. Moreover, the air carried along by the jet stream must be removed through adequate openings at the diffuser circumference.
5. At larger wind tunnels the boundary layer is drawn off from the jet chamber wall.

By a suitable rearrangement in the only small wind tunnel remaining in Göttingen, that of 60KW at the Max Planck Institute for Flow Research, the critical spherical number serving as turbulence mirror, $Re_k = \frac{vd}{r}$ of a sphere with d = 17.5 cm dia was improved from $Re_k = 300{,}000^r$ to 385,000, and a very low turbulence factor TF = 405,000/385,000 = 1.05 achieved. The characteristic spherical numbers of various wind tunnels may be compared by measurements of spheres of equal diameter and equal surface roughness. In the Göttinger wind tunnel a smaller sphere of 12 cm dia reaches an $Re_k = 393{,}000$.

These critical characteristic spherical numbers at the transition from subcritical, laminar detached flow to turbulent attached flow (Fig. 1), are calculated from velocity v when pressure coefficient (p/q = 0) passes through the zero point, measured at the backside of the sphere relative to the maximum Re-number 405,000 obtained by Hoerner [4] from towing tests in still air. According to more recent tests the ideal value Re_k = 410,000 for still air. These Re-numbers of pressure measurements are about 20,000 higher than those agreed upon critical Re-numbers of the sphere from resistance measurements when passing C_w = 0.3 which, according to Platt [5] should agree with the Re-numbers calculated at p/q = -0.22.

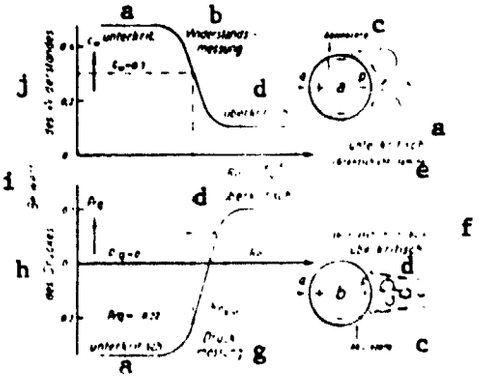

Fig. 1. Definition of the critical Re-number Re_K of the sphere separation zone for the drag number C_W = 0.3 and for pressure measurement p/q = 0.

Key:
a - subcritical
b - Drag measurement
c - Separation zone
d - hypercritical
e - (Laminar boundary layer)
f - (Turbulent boundary layer)
g - Pressure measurement
h - of pressure
i - coefficient
j - of drag

While the shift in the wind tunnel behind a turbulence screen occurs already at Re ≈ 100,000 for the 17.5 cm sphere, Hoerner found Re_k = 380,000 during tow tests in gusty air in areas with trees, which is an only slightly lower value for Re_k than that in still air. That means that the large turbulence ground effects of the free atmosphere have only a very small impact on the boundary of a few millimeters thickness. Strictly speaking, only measurements in turbulence-free air flow result in correct values comparable to free flight. This holds true especially for measurements at at low Re-numbers since at turbulent air flow the subcritical, laminar condition does not appear at all and the airfoil coefficients appear very

much changed. When the low turbulence condition is reached one can easily achieve turbulence for the entire air flow by appropriate measures or one can apply local turbulence inducers on the test body to demonstrate the extremely changeable scale of turbulence effects at low Re-numbers.

Velocity and turbulence distribution may be made extremely homogeneous by inserting fine screens. To be sure the screens transform a considerable part of the compressor power into heat. At each measurement location the temperature change of the air flow (measured at the back of the sphere) must be considered, since otherwise the temperature increase for each degree results in an increase of the Re-number by 2,000, and with increasing and decreasing velocity hysteresis a deceptively wrong Re_k of, for instance, over 430,000 may appear, especially for small spheres.

The following condition is here referred to: it is known that all wind tunnels show troubling resonance oscillations at certain velocity regions (especially wind tunnels with thin sheet metal walls and too small a collecting cone), which increases the turbulence in these regions. It is desirable, therefore, that instead of the critical sphere coefficient, which indicates the exact turbulence condition only at one certain velocity, the turbulence be ascertained for all /151 velocities. Up to now only the measuring method by means of electric hot-wire probes, in conjunction with an oscilloscope as introduced by Dryden, has provided progress. This method allows measurement of the distribution of the turbulence force along the entire

velocity range of a wind tunnel. Low turbulence wind tunnels have a

$$\text{turbulence coefficient } Tu = \sqrt{\overline{u}^2}\ v = 0.3^0/_{00} \text{ to } 1^0/_{00},$$

where u represents the turbulent oscillation velocity, the dash the temporary mean value formation and v the velocity of the basic air flow [6].

The connection between spherical and hot-wire measurements derives from the product of the degree of turbulence and Taylor's parameter

$$Re_k = f[C\sqrt{\overline{u}^2}/v) \cdot (D\ L)^{1/5}].$$

D denotes the spherical diameter and L the vortex ball size derived by means of the two-wire probe. Accordingly, Re_k changes only with the 5^{th} root of D, resp. the change of $\frac{\sqrt{\overline{u}^2}}{v}$ is 5 times more effective than a change of D and L.

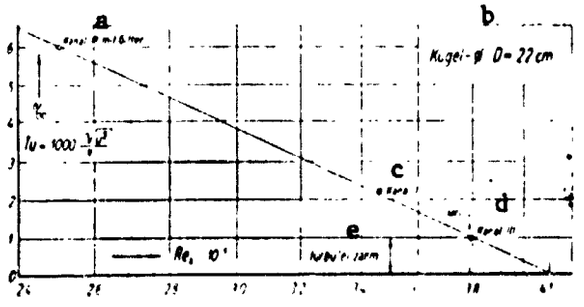

Key: a - Channel III with sieve
b - Sphere diameter
c - Channel I
d - Channel III
e - turbulence poor

Figure 2. Calibration diagram for determination of turbulence coefficient Tu from the characteristic spherical number Re_k. Based on comparison measurements and calculated for a vortex size L = 1 cm; Tu = 0 denotes Re_k = 411,000 (from R. Seiferth).

Figure 2 shows a calibration diagram by R. Seiferth [7], which was derived from comparison measurements by means of a hot wire and a calibration sphere of 22 cm dia. For the small Göttingen wind tunnel, with an elliptic jet of 730 x 1045 mm, a sphere of 220 mm dia would already result in too large a jet resistance. The Re_k number 385,000 for a sphere of 175 mm dia agrees with a turbulence coefficient of $1^0/_{00}$ for this Gottinger wind tunnel, when extrapolated to 220 mm according to Fig. 2.

To measure the effectively small forces at low Re-numbers of the model airplane (10,000 to 200,000) the three component balance must indicate 1/10 of a gram and the dynamic airspeed indicator 1/100 of a millimeter pressure differentials. The velocity must also be capable of very fine regulation between 1 and 10 m/s, i.e., between 0.06 and 6 mm water column. Moreover, to obtain a continuous series of Re-number measurements in a more accurate way for airfoil measurements at low Re-numbers, e.g. in the desired region of 10,000 to 200,000, for model and bird flight and to reduce the scattering of data points instead of the usual "Polar measurements with gradual increase of the angle of attack α at constant velocity," the velocity is gradually increased and decreased with constant α--to obtain the hysteresis loop. In contrast to polar measurements this procedure can be designated as index of measurements. An arrangement of the corresponding c_a and c_w series of measurement vs. Re will result in a random number of polars as cross-sections as shown in Fig. 4.

4. Effect of Turbulence on Spheres and Airfoils

The turbulence effect acting on small airfoils constitutes an analogy to the known boundary layer processes on spheres, which present a clear physical graphic comparison, that was first interpreted by Prandtl. For sphers there exists at the leading edge of flow at the stagnation point a positive pressure (+), while a

negative pressure (-) is directed toward the equator of the sphere by conversion of potential into kinetic energy (Fig. 1). At the backside of the sphere the kinetic energy would change back into pressure (+) without friction loss in a friction-free fluid, i.e. a fluid without viscosity, so that a second stagnation point would appear and the resistance became zero, because front and back pressures would cancel each other. The boundary layer due to the viscosity of the flowing medium is the known reason for all pressure and friction resistance. There are varying flow effects and resistances, depending upon the laminar or turbulent boundary layer flow.

a. The furthest from the ideal form of the friction free fluid is the laminar (= subcritical) boundary layer condition, since the flow is already detached at the equator, because the laminar boundary layer cannot overcome the pressure increase from (-) to (+), which starts there.

b. At a certain critical velocity, resp. Re_k-number, the boundary layer at the leading edge of the sphere will get turbulent by itself after a short laminar start, when a completely smooth sphere is exposed to turbulence-free incident flow at Re = 410,000. The transition zone now lies ahead of the detachment zone; the laminar start will get shorter with increasing velocity. The turbulent (= hypercritical) boundary layer flow has the curious quality, by virtue of fine eddies, to transport energy from the outer flow layer to the one close to the wall, which is slowed down by friction. It can therefore partly overcome the pressure increase at the back side, the flow reattaches itself and in the now much smaller area of eddies there is excess pressure and the drag coefficient c_w decreases from 0.48 to about 0.08, that is to 1/6 (Fig. 1b). This increase in the hypercritical flow condition is due the turbulence effect.

c. The conversion laminar/turbulent may be forced by a "turbulator" even at low Re-numbers, e.g., by attaching a wire ring at the incident flow side of the sphere in front of the detachment zone, which is how Prandtl proved that it depends only on the turbulent boundary layer. The same effect results from a rough surface, or from an already turbulent incident flow. Sonic vibrations (strong whistle tone) may also reduce Re_k, most effectively by turbulence grids made from rods of adequate thickness.

These three conditions can be observed well at any water pipe. (a) If one turns the faucet on slowly, the water flow is at first smooth as glass; the flow is laminar. (b) When opening the faucet a bit further, the water flow suddenly turns turbulent at a certain critical velocity. (c) If one holds a needle in the laminar stream, then the flow is turbulent from that point on.

The conversion laminar/turbulent occurs on airfoils at much /152
lower Re-numbers than on the sphere and it occurs on thin, flat plates already at Re ≈ 10,000, corresponding to the gliding flight of large butterflies and small hangar airplane models. At turbulence-free incident flow the conversion starts at Re ≈ 100,000 for round nosed-thick profiles of 20% thickness and reaches full turbulence at about Re ≈ 150,000, which corresponds to the flight of very large gliders and large birds.

In Fig. 3 the result of a wind tunnel measurement on an airfoil with the profile N60 at $\alpha = 30$ is presented as an example. In the subcritical condition the laminar boundary layer of the upper surface of the profile detaches itself since it cannot overcome the locally starting pressure increase (Fig. a).

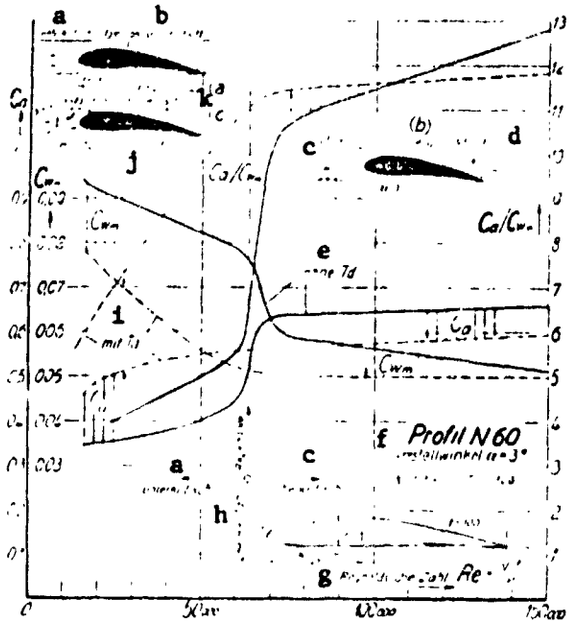

Fig. 3. Result of an airfoil measurement for profile N60 at an angle of attack of 3 up to a Reynolds number of 150,000. Dotted line: with prepositioned turbulence wire Td. Solid line: without turbulence wire.

Key: a - subcritical
b - laminar boundary layer
c - hypercritical
d - turbulent boundary layer
e - without
f - angle of attack
g - Reynolds number
h - critical Re-number
i - with
j - with 0.70 turbulence wire
k - turbulent boundary layer

At the profile N60 the critical Re-number is 63,000. With increasing suction of the flow at the upper surface the stagnation point moves towards the airfoil's lower surface. From the stagnation point on the boundary layer flowing towards the airfoil's upper surface receives the larger a centrifugal force ($Z = \rho \cdot v^2/r$), the smaller the nose radius r becomes, causing the boundary layer to become turbulent and the point of attachment to move downstream (Fig. 6). The drag coefficient c_w decreases from 0.09 to 0.05, the lift coefficient c_a increases from 0.35 to 0.65, the lift/drag ratio c_a/c_w from 4 to 13; the airfoil now reaches three times the gliding distance.

Consequence: An airfoil model will attain optimum performance in accordance with its size classification only in the hypercritical condition. These requirements can always be met: (1) by suitable

choice of profile, or (2) by means of artificial turbulence, e.g., by adding a prestressed cable as a turbulator (Fig. c), causing the boundary layer for profile N60 to become hypercritical already at Re ≈ 20,000.

5. The Hysteresis Loop

In the hypercritical condition the air force-measurement shows hysteresis after separation of the flow in the stall condition with decreasing α, which broadens very undesirably at a high Re-number even for thick airfoil profiles, and at low Re-numbers especially at turbulence-poor flow even for medium thick airfoil profiles. As explained in chapter 3, the "index measuring method (α = constant, v = variable)" attains more accurate measurements for low Re-numbers than the usual "polar measurement (v = constant, α = variable)." To comprehend the hysteresis correctly with the index measuring method the flow must be set up hypercritically for large angles of attack, when reaching the desired highest velocity, by placing a cane in front of the airfoil leading edge, in case the flow does not become hypercritical on its own, so that the $c_{a\ max}$-value, resp. the upper branch of the hysteresis square, appears (CGH in Fig. 4), e.g., for the profile N60 according to Fig. 5 for $R_e \approx 160{,}000$ above α = 10. This curiously different behavior of a profile during the two measuring procedures is caused by the movement of the stagnation point, whose course, at constant α and decreasing v, is conforming only with the course for the polar measurement method and with free flight when "originating from the hypercritical condition." On the free flight model the flight mechanical interpretation of hysteresis after separation of the hypercritical flow due to a gust or a calm is visually observable, with the model pitching down at smaller α, flying faster until the flow at the "initial angle of attack" and at higher Re-number reattaches itself hypercritically, thus restoring the normal glider flight position.

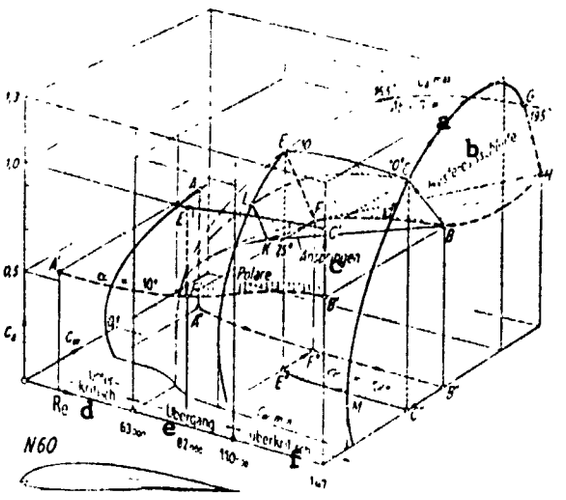

Fig. 4. Three-dimensional coordinate system c_a vs. c_w and Re for presentation of the connection between the characteristics measurement method (longitudinal section) and the polar measurement method (cross-section) on profile N60 for $\alpha = 10^o$.

Key: a - Separation
b - Hysteresis loop
c - startup
d - subcritical
e - Transition
f - hypercritical

Thin, flat and slightly curved surfaces show in the here measured region Re > 2000 no subcritical condition and no hysteresis, which is also true for medium thickness airfoils, e.g.,N60 when a pre-stressed turbulence string secures the hypercritical condition.

6. The Leading String as Turbulator

In Fig. 5 the envelope curve of the separation points is identical with the steeply increasing $C_{a\ max}$ line which, emanating for N60 from $Re_k = 63{,}000$, after a transition region at 110,000 with $\alpha = 17$, /153 reaches a $c_{a\ max}$ of 1.3. The boundary layer at the airfoil's upper surface is now fully turbulent due to increasing "foil leading edge turbulence" (centrifugal acceleration due to movement of the stagnation point) and adequate drag effect of the outer flow, i.e., adequate transport of energy in the boundary layer. The effective region of the turbulence effect ends here with the achievement of full turbulence, including the obtainable advantage through means of artificial turbulence through a tripping ledge, leading string, surface roughness, turbulence edge, etc. The limits of effectiveness of a turbulator at low Re-numbers remain unknown since even insect wings of only 1mm length, surrounded by fine hairs, are probably still operating in the sense of the turbulence effect in the, for them, almust mushy fluid "air."

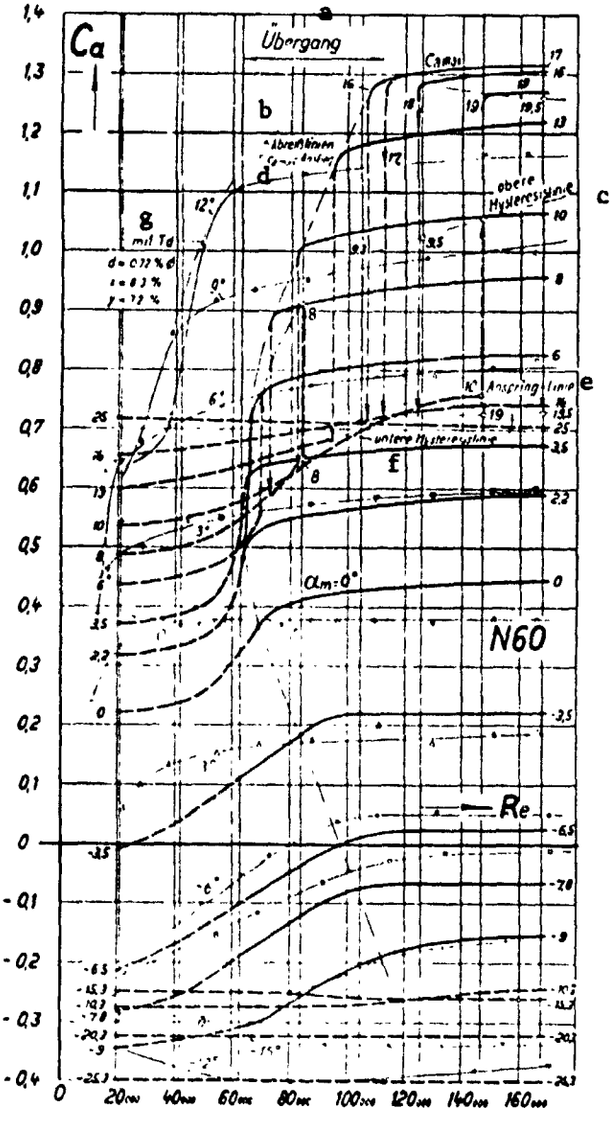

Fig. 5. Results of measurements on air foil N60: Plot c_a vs. Re α_n is the measured angle of attack (without calculated correction). For comparison the turbulence effect for the four angles of attack already active at Re = 20,000 due to the turbulence string (Td fastened to the model) is shown.

Key: a - Transition
b - Separation lines
c - upper hysteresis line
d - rise
e - starting line
f - lower hysteresis line
g - with

On flight model airfoils the obtainable advantage of a turbulator is, e.g., that with a leading wire, the hypercritical condition may be achieved already at a considerably lower Re-number. For profile N60 the separation line is advanced approximately equidistant by a Re-number range of 40,000, from 63,000 to 20,000 (for a 20% thick airfoil even from 105,000 to 200,000). The flow separates itself from profile N60 for Re = 20,000 at α = 7, but at 40,000 a c_a of 0.9 with a 9° angle may be achieved and a c_a of 1.1 with 12° at 60,000, instead of at 90,000. The turbulence string (fishing line or rubber band) must be at least 0.4 mm thick, is pulled tight at a certain spot ahead of the stagnation point and is then fastened with about 25 cm support distance. In Fig. 3c, the arrangement of this string of 0.7 mm dia in front of a model with 90 mm profile depth is shown in percentages of t. The gain obtained by means of this turbulence string (Td) is drawn as a dashed line.

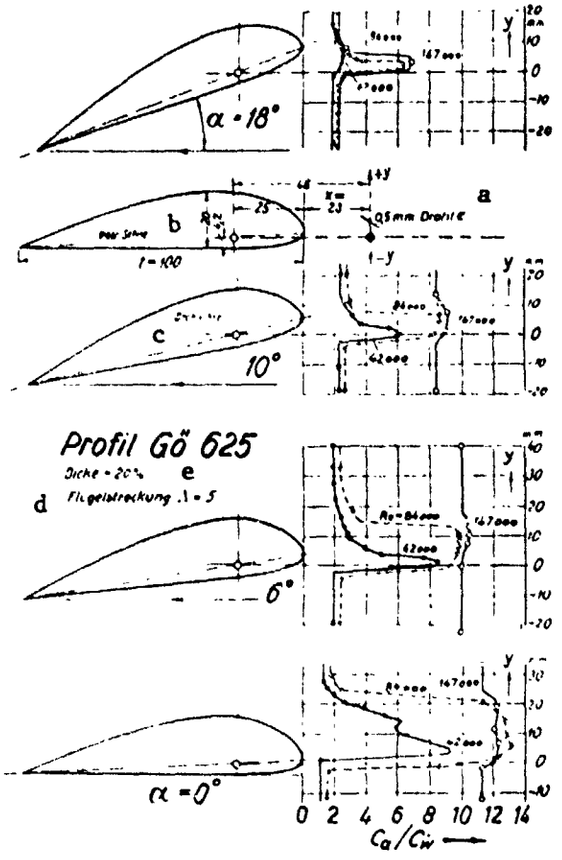

Fig. 6. Results of measurements to judge the effect of elevation of the turbulence wire on the thick, round-nosed profile 625.

Key: a - wire dia
b - chord
c - Turning axis
d - Aspect ratio
e - thickness

For Re ≈ 50,000, for instance, c_a is greater by 38%, c_{wm} is smaller by 33% and the glide coefficient is improved from 5 to 10. In comparative measurements with other turbulators the leading string proved to be most effective on a normal airfoil in the region of Re ≈ 30,000 to 100,000; below 30,000 a tripping edge of 1 mm above the profile's leading edge was more advantageous.

For tests of the elevation of a turbulence wire the 20% thick airfoil GÖ 625 was chosen, which is very turbulence-sensitive due to its large nose radius of 3.4%. In Fig. 6 the c_a/c_w values of the wind tunnel measurements on the model with aspect ratio 5 are presented for five different angles of attack and three different Re-numbers, as function of the elevation of the turbulence wire.

The wire of 0.5 mm dia is not attached to the model, so that its resistance must be considered in the application. For evaluation of the effect it is noted that the critical reversal for profile 625 without turbulence wire starts at Re ≈ 105,000 and reaches full turbulence at 155,000; but it starts already at 20,000 with a turbulence wire and at 70,000 operates completely hypercritical.

At α = 0 and Re ≈ 84,000 the wire yields an extraordinary improvement of the glide coefficient from 2 to 13 and this in a large vertical effective range Y from 0 to 20% t above the axis of rotation. For Re ≈ 42,000 the wire produces a maximum value of 9 only at a certain elevation of Y = 5%.

With increasing angle of attack the vertical tolerance field gets smaller and moves downward, as the c_a/c_w point for 42,000 shows. This is explained by concurrence with the movement of the stagnation point downward around the airfoil nose (Fig. 7).

Optimal affect should be obtained for the model up to the stalled flight condition at 18°, if the wire were turned by a swivel device by about the same angle downward around the t/4 turning point. At 18° the effect of Re ≈ 42,000 remains only small, but up to complete characteristic turbulence at Re ≈ 155,000 still quite favorable. From further tests on profile 625 it was found that with reduction of the horizontal distance to about 10% a wire of 1 mm dia, attached solidly at an elevation of 8%, produced a similar favorable effect. A wire of only 0.2 mm dia became only effective when it was oscillated, which in practice corresponds to a thickening. /154

7. Airfoil Nose and Movement of the Stagnation Point

The boundary layer flow at rounded bodies is more prone to turbulence and more dependent on the Re-number than on rounded bodies with edges on the incident flow side. Such tripping ledges provide, even for airfoils at Re < 30,000, a useful turbulence effect when used appropriately in the region of low Re-numbers--as on a sphere--when too large they act as separating edge on the airfoil!

At the leading edge of an airfoil there are, besides the premise of turbulence-free incident flow, the following parameters of relevance: the motion of the stagnation point, the form of the leading edge (nose radius r, intake angle ψ of the airfoil center line, the increase in thickness along the airfoil center line), surface roughness, the angle of attack α and the Re-number.

At the well known test of the rotating cylinder in a parallel flow the frontal stagnation point moves against the circulation, the rear one with the circulation. At $u/v = 4$ both points coincide [2], the body is completely sucked into the low pressure regime. At the airfoil the lift is proportional to the circulation, so that with increased lift even here the stagnation point is moving counter to the circulation around the profile nose towards the airfoil underside. In Fig. 7 this stagnation point movement is presented on two profiles [1] from the Göttingen pressure measurements. Although this stagnation point movement along the pressure side of the wing amounts to only a few hundredths of the profile depth, it has considerable influence on the turbulence of the motion side boundary layer, which is the greater, the smaller the nose radius is.

For the pointed nose profile 389 (Fig. 7) a pressure drop exists at $\alpha = 14.6°$ from the stagnation point to the pressure minimum, which is only about 4 mm away, equalling 4.7 times the velocity pressure, so that the velocity at the free border of the boundary layer is accelerated from 0 to 64 m/s in 1/8000 second. This acceleration of 512,000 m/s^2 is greater than that of a bullet. For the thick profile 282 at $\alpha = 14.5$ velocity rises from the stagnation point to 34 m/s along a distance of 7 mm in 1/2000 s. The acceleration here is only 87,000 m/s^2, which is less than 1/6 of that for the thin profile. The pressure minimum, however, lies further above the profile nose where from the stagnation point on $v_{max} = 55$ m/s is reached after 38 mm distance, while for the thin profile an enormous pressure increase starts at the suction point close to the front edge where the velocity already starts to decrease.

The larger acceleration of the boundary layer at the pointed nose profile explains why the laminar/turbulant transition for it starts at a low Re-number--as on profile N60 at about 63,000--while for the thick **round-nosed** profile 625 the transition only occurs at Re = 105,000! This leads to the conclusion that the boundary layer should flow around the knifelike leading edge of a flat plate (nose radius $r > 0$) with a theoretically infinitely large velocity since the mass point , which moves with velocity v from the radius r on a curved trajectory, is exposed to a centrifugal force $Z = \frac{v^2}{r}$. Instead the boundary layer detaches itself from the leading edge and forms a stationary transition vortex at whose backside the airflow becomes turbulent and r attaches itself. This transition vortex propagates with increasing angle of attack, with the upper boundary layer functioning somewhat like a curved, fluid profile side. Once /156
the transition point was reached the rear edge involute, vortices are formed in the stationary transition vortex **which, increase**

rapidly and then flow away. The flow then detaches itself after strong incident shocks at angle of attack of 5-10. The edge of turbulence now becomes the detachment edge. For as with all profiles the separation proceeds from the rear edge to the leading edge. For the functional profile the events are the same, only they are distributed over a wider angle of attack range due to the curvature of the nose and camber of the wall.

Flat plates and thin symmetrical profiles are not pressure point sensitive from -6° to +6°; the pressure point lies at t/4 and for larger angles of attack it moves towards the rear edge. Prior to "stalling" it acts in the sense of automatic longitudinal stabilization if one trims the center of gravity to 28% of the plate thickness with a postcard according to the example of the "flying board" by Lanchester [8]. Flat plates reach only a c_a of 0.5 for Re ≈ 20,000 and 0.6 at Re ≈ 168,000 and 0.7 at Re ≈ 420,000; flat plates do act alreay hypercritical at Re = 10,000, the air flow detaches itself already at a small angle of attack and, therefore, attains only those small values of c_a.

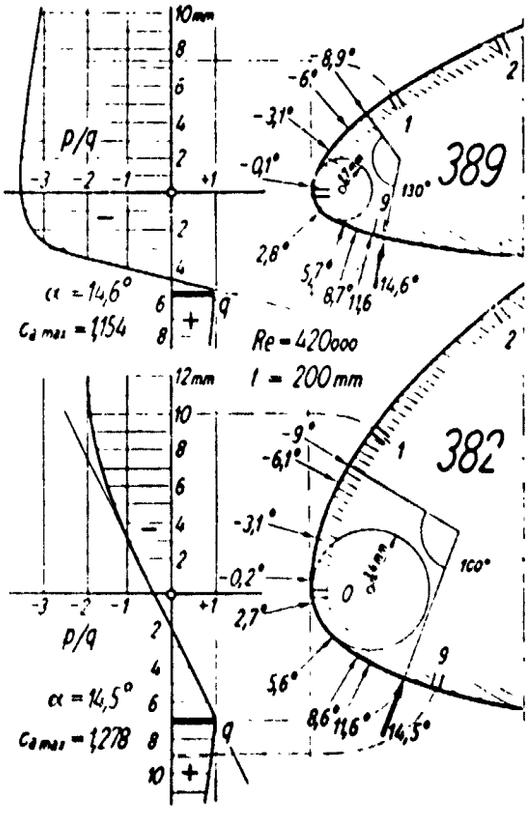

Fig. 7. Movement of the stagnation point and pressure distribution for a profile with a pointed nose and one with a round nose.

8. Description of Airfoil Tests on Profile N60

The results of the three component measurements on profiles

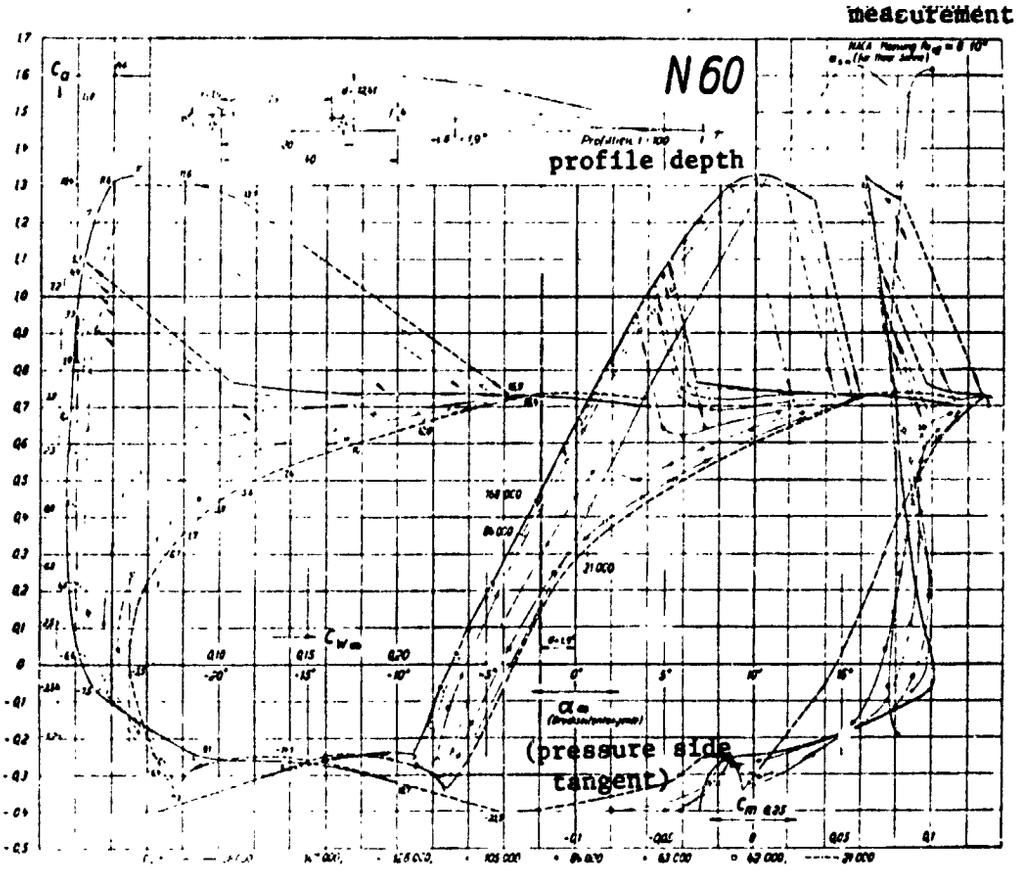

Fig. 8. Test results of profile N60: curve c vs. $c_{w\infty}\alpha^{\infty}$ and $c_{m0.25}$

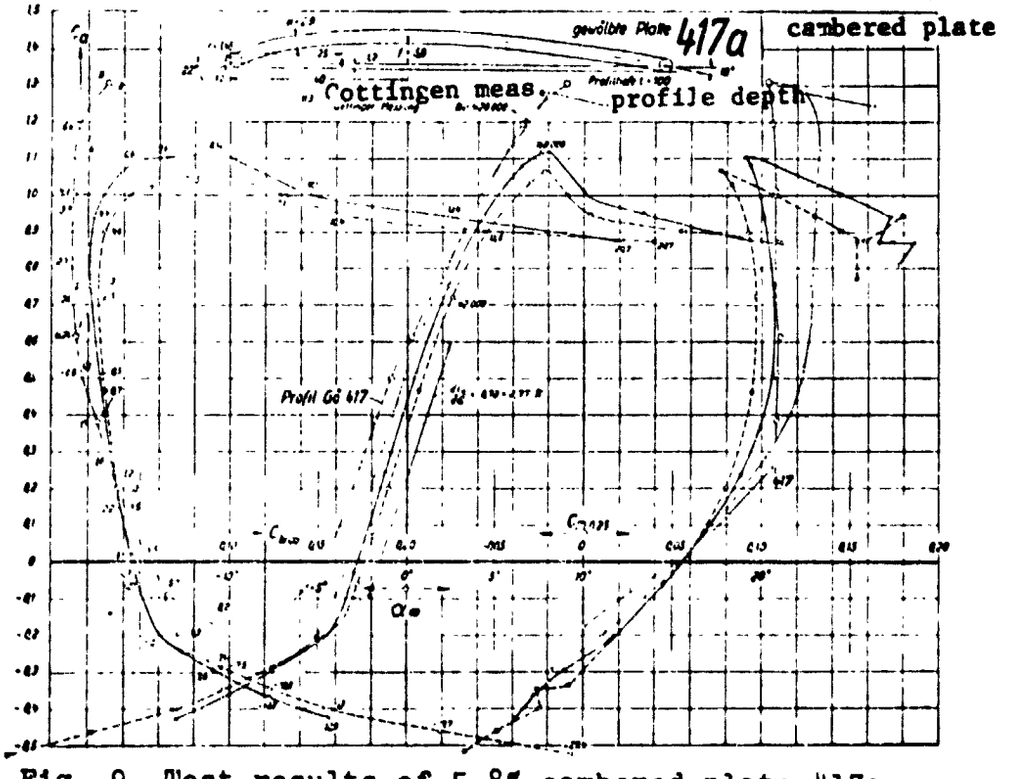

ORIGINAL PAGE IS
OF POOR QUALITY

Fig. 9. Test results of 5.8% cambered plate 417a: c_a vs. $c_{w\infty}\alpha_{\infty}$ and $c_{m0.25}$

N60, 417a and 417b, are presented in diagrams 8-14 by plotting c_a versus $c_{w\infty}$, α_∞ and $c_{m0.25}$ The indices ∞ indicate, that the drag measured on rectangular airfoils of aspect ratio A = 450:90 = 5, c_{wm} was transformed into an infinite wing aspect ratio after treating the finite flow of the wind tunnel with the Betz formulas--according to Prandtl's airfoil theory--taking into consideration the transition from a rectangular to an elliptical wing. The coefficient $c_{w\infty}$ represents the remaining profile drag after deduction of the induced drag.

The NACA-profile N60 is shown in Fig. 8 by test values for 8 different Re-numbers from 21,000 to 168,000. In addition, the NACA test data at $Re_{eff} = 8.10^6$ is shown for comparison. In the subcritical region <63,000 the lift is small and the drag large with the moment coefficient $c_{m0.25}$ (referred to the pressure axis at 0.25 t) very variable. The curves for Re ~ 84,000 are still in the transition region to the hypercritical boundary layer flow. At 105,000 with full turbulent boundary layer $c_a = 1.25$ is reached and the flow separates only at $\alpha = 9.5°$. The flow cannot be more than fully turbulent so that the drag effect of the outer flow alone can affect only a small, but constant, improvement of the flow corresponding to the energy content increasing with the Re-number. The polar does not separate any longer in a sharp point, but rather after a soft transition. The moment line $c_{m0.25}$ shows the customary S-curve and hypercritically an average value of 0.08.

9. The Cambered Plate 417a (f/t = 0.058)

In contrast to profile N60 the influence of the Re-number on thin cambered plates is very small; the polar diagrams of R = 42,000 and 168,000 in Fig. 9 show only small differences. The Göttingen polar [1], shown here for comparison as tested at Re = 420,000, reaches an only slightly higher maximum lift, as is true of profile

417 which is similar to the cross-section of a bird wing. For a camber of 5.8% this thin plate generates a large lift already at 0.

For good gliding qualities a model requires a high lift coefficient $c_a \approx 1$ and low airfoil drag in this region. Both apply to the cambered plate. For Re = 42,000 the best glide coefficient of a glider model 417a for an aspect ratio A = 10 is about 14 according to Fig. 16. Moreover, the airfoil (Fig. 9) shows, after passing the maximum lift, no sudden decrease to a subcritical value as for N60, but only a small decrease even for very large angles of attack. The large drag at $c_a = 0$ is not undesirable as reduction of the driving velocity. On the other hand, the large center line camber of 5.8% causes larger stagnation point movement, as seen from the moment line. This means that a larger control surface is required for longitudinal stability, while the flat plate is inherently stable in flight when the center of gravity is positioned correctly.

The advantage of thin cambered plates in the Re-number region up to 100,000 is based on three reasons:

1. The advantageous cooperation of the tangential incident flow at the leading edge at large angles of attack with the turbulence effect of the small nose radius;

2. The strongly concave underside, which shares significantly in lift generation; and

3. The comparatively small camber of the airfoil's top side, causing the flow to remain largely attached.

The motions of the stagnation point controls events even here in combination with the frontal turbulence. In contrast to profile N60, where after detachment of the flow the boundary layer at the front of the profile (nose) is laminar, i.e., subcritical, the leading edge maintains the flow here continuously turbulent. For

large negative angles of attack the flow at the underside separates. At -5° it attaches itself partly to a transition vortex reaching up to the leading edge. At an angle of attack of about -3° the transition vortex shrinks beneath the leading edge, reducing the drag and making the pressure distribution more complete. Only now can the stagnation point move underneath the leading edge, making the transition vortex disappear and the upper flow become turbulent. With increasing angle of attack the increase in lift $d\, c_a/d\bar{\alpha}_\infty$ results in a high value of 2.77π, which even surpasses the increase in lift of 2π for a flat plate. For the model airplane this does mean "gust sensitivity," however.

For practical applications it is, of course, recommended, to streamline the airfoil section, i.e., to shape the wing rear edge like a knife edge in place of the uniform thickness of the metal plate in the wind tunnel model 417a.

10. The Cambered Plate 417b (f/t = 0.087)

For small light hangar flight models whose wings are formed by a cambered film skin supported by thin aluminum wires and which fly at Re < 20,000, the camber of plate 417a proved to be too small. With a camber of about 8 to 9% of the wing depth t much better results were obtained. Due to this observation a more curved metal plate with the parameters f/t = 0.087 at 0.4 t and d/t = 0.035 was tested in the wind tunnel. Results were surprising.

1. While plate 417a with 2.9% less camber proved to be turbulence-insensitive in the tested Re-region, with the plotting of c_a and c_w vs. Re resulting in almost horizontal lines, the more cambered plate 417b was turbulence insensitive only at Re > 100,000 (Fig. 10). /157

2. The c_a lines show a definite minimum at Re = 42,000, which up to now was not observed at any airfoil. While for all

Intermediary condition -

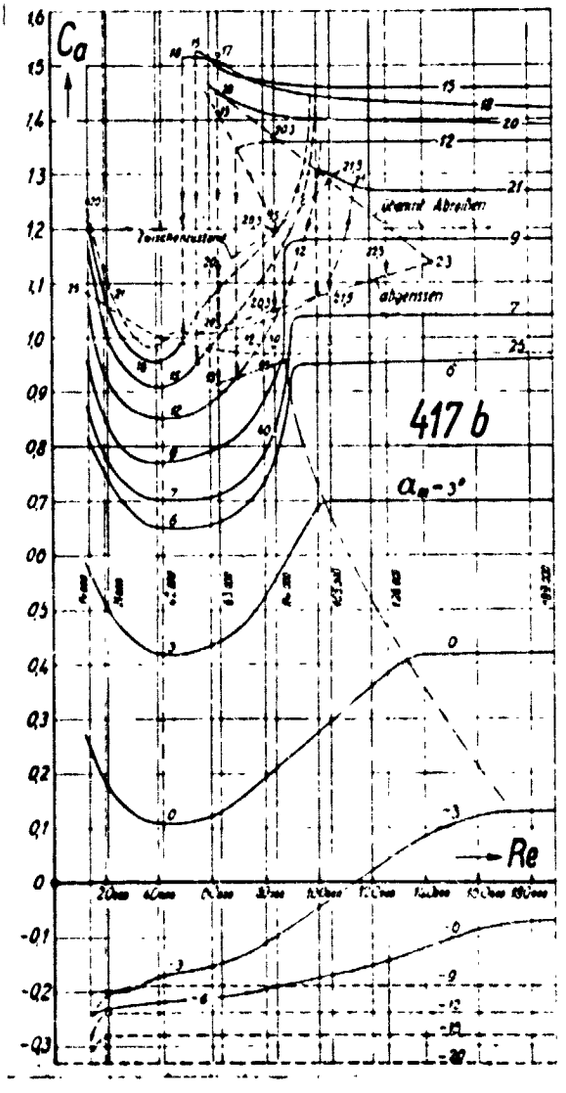

-hypercrit. separation

-separated

Fig. 10 Test results of the 8.7 % cambered plate 417 b ca vs. Re

standard air foil profil-s the hypercritical flight condition on models is only dependent on the upper boundary layer, which is resp. dependent on the frontal turbulence, (the influence of the bottomside flow--whether laminar or turbulent--is very small), the picture is quite different for the more curved plate due to inhibition of the motion of the stagnation point. Because of the extremely large incident angle $\psi = 31°$ (see Fig. 13) a stationary transition vortex is effective in the Re-region around 42,000 up to the separation angle of attack of $\alpha = 21°$ underneath the wing leading edge, whose suction pressure does not permit the stagnation point to advance towards the bottom side, so that the upper flow is subcritically detached, or remains in the semiturbulent transitory conditions while the bottomside flow is attached behind the transition vortex. In this way the air mass, which is directed towards the bottom at the underside, still generates lift at Re = 42,000, which is only a little less than for 417a, but with considerable drag, e.g., at $\alpha_m = 6°$ double the amount ($c_{wm} = 0.13$ at $c_a = 0.65$).

3. With increasing R_e-numbers the top side flow only reaches fully hypercritical condition for small angles of attack, i.e., small stagnation point motion as for N60, only for higher Re-numbers, e.g., for 0° at Re = 140,000. To the right of this rising dashed and dotted line in Fig. 10 the c_a-values remain hypercritical and constant in agreement with the c_{wm}-lines of Fig. 11 where, from 7° on at 100,000 to 13° at 63,000, small C_w-jumps with hysteresis indicate a stepwise change of the transition vortex at the bottom side; these events are visible in Fig. 10, above $c_a = 0.9$ between 63,000 and 105,000, as incidence zone (dashed and dotted triangle).

4. Beyond this region, for larger angles of attack, resp. Re-numbers, the stagnation point has moved so far towards the

bottomside, that the upper airfoil flow, in starting to become turbulent, helps to control the following events. The simultaneous dependence of top and bottom side flow creates a situation where for 18° to 21.5°, from R_e = 50,000 to 105,000, three flow conditions are possible for every detachment angle of attack, which in Figs. 10 and 11 are defined by three lines as "hypercritical detachment," "intermediate condition " and "flow detached."

5. The characteristic decrease of the c_W-lines at R_e = 14,000 to 42,000 is to be understood in such a way that at the beginning of the "creeping-attached flow" the transition vortex is not yet developed, that its turbulent energy absorption then increases rapidly and at $R_e \approx 42{,}000$ reaches maximum effectiveness in relation to the subcritical top side flow.

6. The hysteresis loops in Figs. 10 and 11 show sharply delineated detachment shifts only when testing with decreasing Re-number, e.g., in Fig. 11, at R_e = 48,000 and 18°, a C_a-shift from 1.5 to 1.0. In contrast to this and to N60 (Fig. 5) attachment of the top side flow occurs with increasing Re-number slowly along a Re-number range, e.g., for 18° from R_e = 48,000 to 98,000, as is also shown by the c_W-lines in Fig. 11.

7. The graphing of the torque number $C_{m0.25}$ shows an extraordinary high value of 0.2 in Fig. 12 for the standard flight regimen at 3° to 12° values for α. Its comparison and practical significance will be discussed in paragraph 9.

8. To summarize: if one compares the lift generation at the cambered plate 417b and at profile N60 by means of Figs. 10 and 5, a similarity of profiles of the c_a-lines is only discernable in the lower part of the figures. There the c_a-lines increase from left to right.

With increasing Re-number and negative pressure at the upper side 417b reaches a constant positive c_a-value at -3°, and Re = 170,000. At larger α a constant hypercritical value is already reached at a lower Re-number, so that the dashed and dotted curve of these values rises from right to left. This represents the limit of influence of the bottom side flow: to the right the c_a-lines run horizontally, indicating the full effect of the upper side flow. While for N60 in Figure 5 this limit of influence of the bottom side flow at c_a = 0.5 and Re_k = 63,000, with the beginning hysteresis as incident line, moves again towards the right, forming a connecting line between the hysteresis quadrangles, this line ends at 417b above c_a = 0.9 in a cluster of upwards curving "attachment lines" for α = 12° to 21°. With the upper, hypercritical, c_a-lines and the vertical line of detachment they form an only 3-sided hysteresis loop. The "startup" of flow is recognized only at 7° to 9.5°. At 9.5° and 84,000 the hysteresis in the starting condition is only a vertical line while the lift shifts from 0.95 to 1.21 and again discontinues at a small Re-number change. It is notable that at this discontinuation a c_a-decrease of 21% with a c_w-increase of only 5% is shown, as is apparent in Figure 11. The c_w-changes during detachment and attachment increase rapidly until the flow at 23° is entirely detached, even at higher Re-number without c_w-shift. /158

The high hypercritical $c_{a\,max}$-values at low Re-number may be evaluated as especially characteristic turbulence effects for profile 417b, since for a decreasing Re-number the flow separates only at the low Re-number of 50,000 with 18°, at the very high c_a of 1.5, with the stagnation point at the airfoil leading edge shifting upward. With the turbulator put in the lead the hypercritical condition may be restored immediately. This condition distinctly explains the creation of hysteresis through motion of the stagnation point in the turbulence-poor airflow, i.e., in agreement with the process on the free flight airfoil model.

9. In the polar diagram of Fig. 13 the test results of profile 417b are arranged converted into an infinite wing aspect ratio. According to the previous explicit interpretation the extraordinary shifts in

the range of Re ≈ 63,000 and 84,000 are understandable. The plotting of c_a vs. α_∞ shows for c_a = 0 - 0.7 a corresponding sudden lift increase of 3π, for Re ≈ 105,000 even an exceptional 7π! The moment lines $c_{m0.25}$ show large increases of the moment of nose-heaviness up to c_a = 0.7 for all Re-numbers, which means an extremely gust-sensitive flight of the model at the concurrent strong lift change in this region. From c_a = 0.7 to 1.4, i.e., around the median value of c_a = 1 at which a glider model generally flies, the torque remains somewhat constant at $c_{m0.25}$ = 0.19. In this case double the torque of the less cambered plate 417a, with c_{ma} = 0.1, must be compensated for in this c_a range.

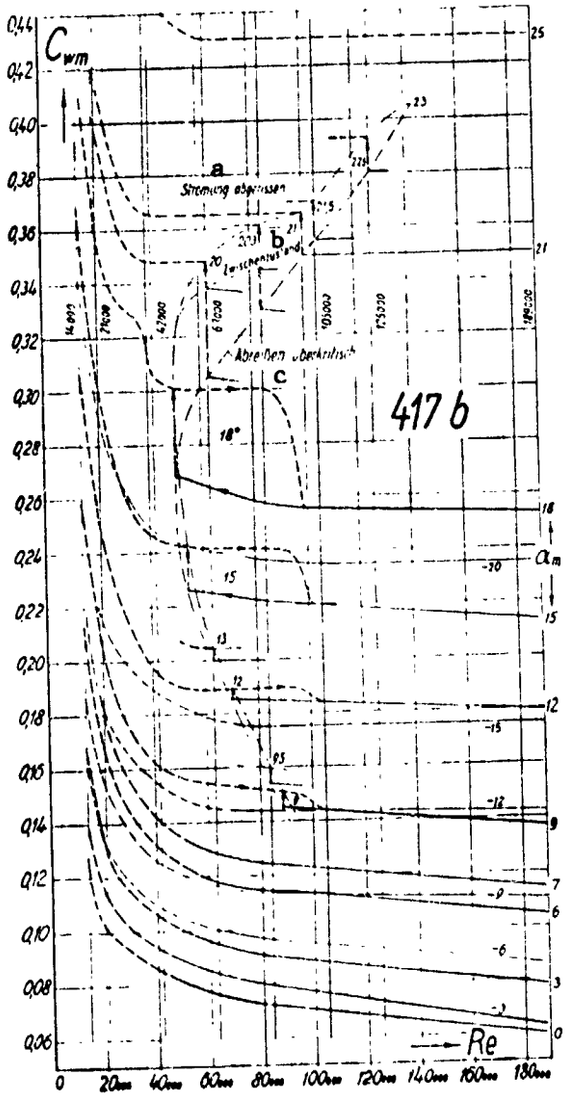

Fig. 11. Test results for plate 417b with 8.7% camber: c_{wm} vs. Re.

Key: a - Flow separated
b - Intermediary condition
c - hypercritical separation

To gain a clear picture of the effective zone of the turbulence effect for profile 417b, the model was then tested in turbulent airflow. Instead of the turbulence screen the turbulent slipstream of a wire of 4 mm dia which was solidly attached horizontally 400 m/m in front of the model in the wind tunnel jet was sufficient.

From the smooth curve of the plotted test results in Figure 14 it can be seen that now all complications of the obstructed stagnation point motion are eliminated. No more subcritical flow condition and no more hysteresis appear. The polar at Re = 14,000 surpasses the others even though the minimum value of the profile drag at c_a = 1.55 is relatively high. /158

The $c_{a\ max}$ values, which decrease with increasing Re-numbers, show that here the turbulence has become excessive. Only below Re = 63,000 is a turbulence effect assured for profile 417b. Beyond this the artificially strongly broadened upper boundary layer leads to earlier separation, which occurs speedily and without hysteresis, the re-attachment occuring then as speedily. The rise in the lift line $dc/d\alpha_\infty$ amounts to about 5π at a Re-number of 14,000 from $c_a = 0$ to about 1.3. The increase of the torque coefficient is, up to $c_a = 0.7$, the same as in Fig. 13. Beyond this the lines run gradually without sudden shifts, so that an airfoil model with a wire attached in front of it has much better flight qualities and is less gust-sensitive than without such a turbulator. Perhaps two wires should be used to keep the upper and lower boundary layers turbulent at the same time over the entire angle of attack range.

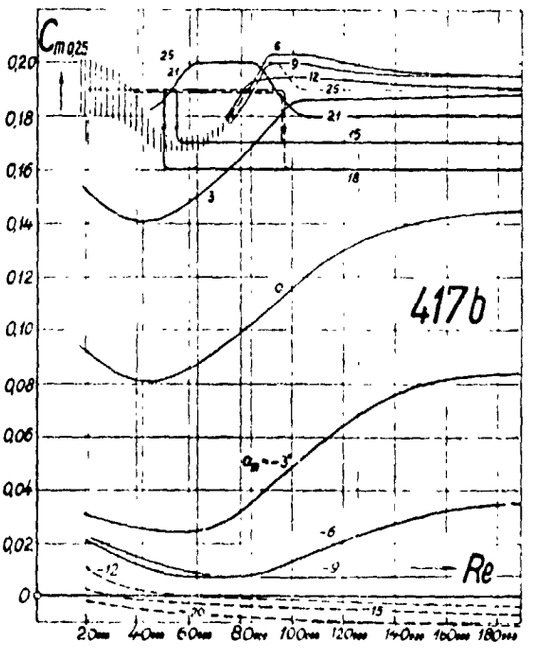

Fig. 12. Test results for plate 417b with 8.7% camber: $c_{m0.25}$ vs. Re.

For a streamlined airfoil profile configuration with parameters (in % of t) r = 1.5, f = 8.4, d = 6.2, slightly more favorable values may be expected. The index numbers present the rearward position of the camber and thickness. For this a string of at least 0.5 mm dia should be applied about 8% in front of the leading edge of the profile at the level of the pressure side tangent. When used without a turbulator, r and f should be kept smaller for optimal effect in the region of Re = 30,000 to 80,000, e.g., r = 0.7 and f ≤ 7.

11. Comparison of Test Results.

By drawing the polar diagrams

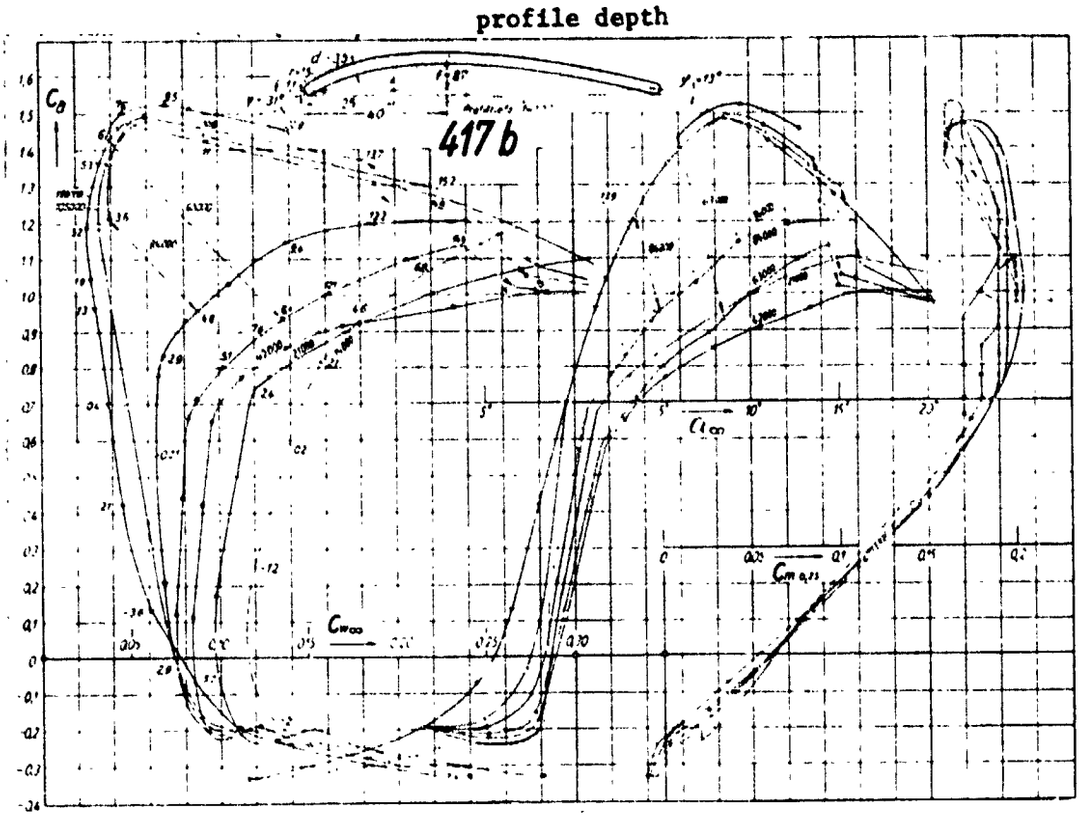

Fig. 13. Test results for plate 417b with 8.7% camber: c_a vs. $c_{w\infty}$ and $c_{m0.25}$.

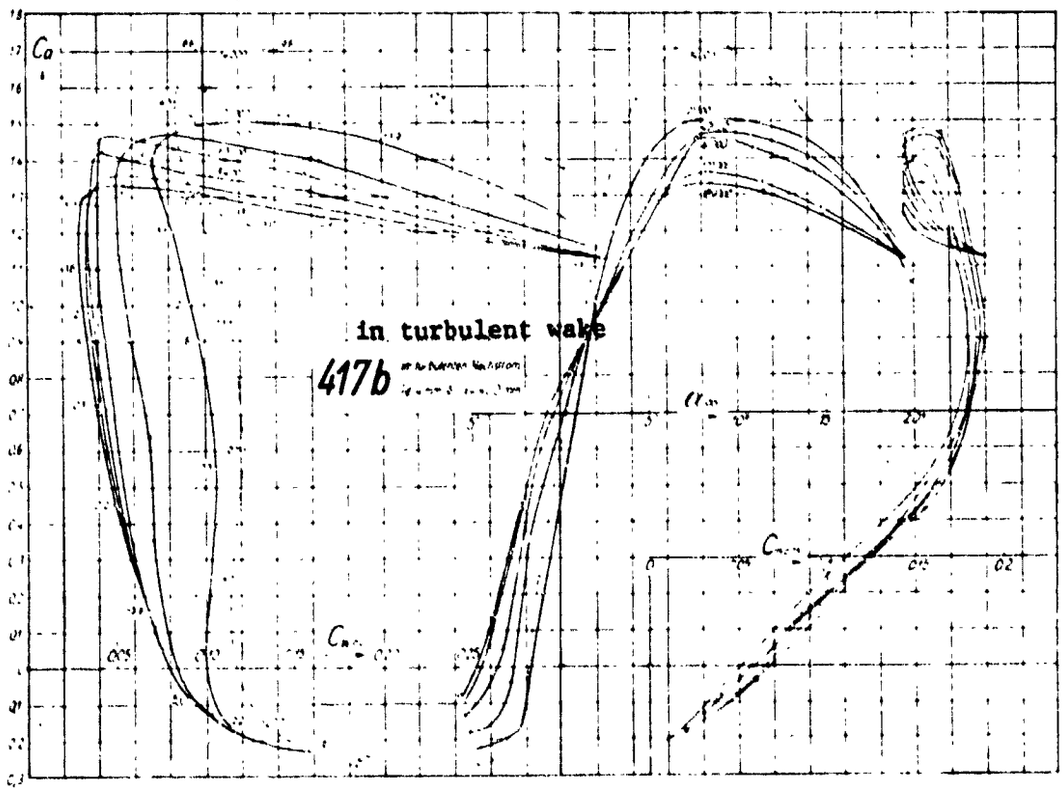

Fig. 14. Test results for plate 417b with 8.7% camber in the turbulent slipstream: c_a vs. $c_{w\infty}$, a_∞, $c_{m0.25}$.

cambered plate

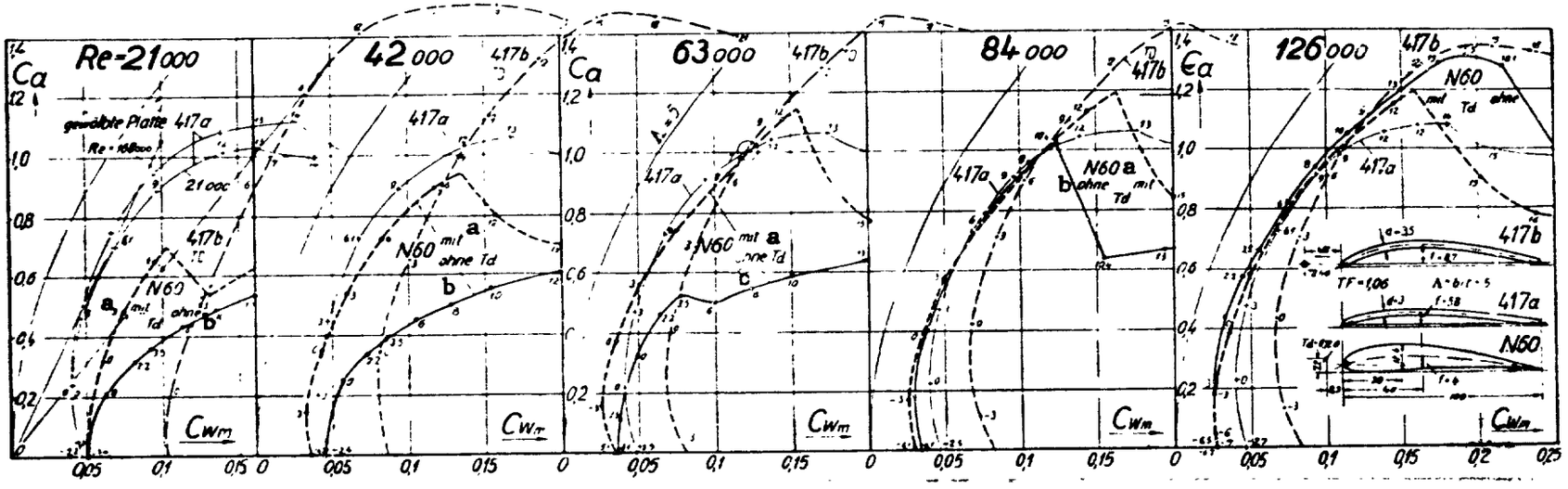

Fig. 15. Comparison of polar diagrams of the three airfoil profiles (N60 with and without turbulence wire, 417a without turbulence wire, 417b with turbulence wire) for five different Re-numbers from 121,000 to 126,000.

Key: a - with b - without

/160

(Fig. 15) of the 3 airfoil profiles N60, 417a and 417b in superposition, one gains an overview of the order of magnitude of various indices of the profiles. The uncorrected test values of the rectangular flight models of the aspect ration A = b/t = 5 are presented, as the index m at C_{wm} indicates. The 3 airfoils are again drawn at the right, 417b being tested in the turbulent wake of a wire of 4 mm dia, which is applied 400 mm in front of the model at the nozzle.

Re = 21,000. Airfoil profile N60 is subcritically very bad and even with a turbulence string it reaches only a c_a of 0.7. The airfoil 417b with 8.7% camber reaches double this c_a value of 1.5 in a turbulent airflow, but it is inferior to the plate with 5.8% camber due to its very large drag. As can be read at the intersection of the tangential pole line at c_{wm} = 0.1, 417a reaches the best glide ratio c_a/c_w = 10.5. while 417b only reaches 6.2. Moreover, 417 is almost insensitive to a change of the Re-number, as the barely more efficient polar at Re = 168,000 demonstrates impressively. At 417a a test with the string fastened in front of the airfoil or in turbulent airflow, resulted in no improvement, like on airfoil 417b.

Re = 63,000. For airfoil profile N60 the transition from subcritical to hypercritical condition begins here. With Td it has at c_a = 1 the same values for 417a as for 417b.

Re = 84,000. The polar plots for 417a and N60 are identical to c_a = 1 where N60 without Td separates at 10.4°; with Td it reaches c_a = 1.2 at 13°C. The cambered plates do not detach with large c_a decreases but with a gentle transition: 417a at 13° for c_a = 1.07, 417b only at 15° for c_a = 1.42. For small angles of attack 417b has, however, a lower diving speed than the others due to its large drag.

Re = 126,000. At this Re-number the limit of the effective range of the turbulence effect for profile N60 is already exceeded, since it /161
not only reaches a higher $c_{a\ max}$ = 1.3 without Td, against 1.2 with Td, but has also a lower drag.

Above this Re-number range the wire applied in front of the foil even results in a somewhat larger drag and a lower lift maximum. Consequently, all airfoil measurements where a V-wire was mounted horizontally in front of the airfoil model for drag measurement (to save a second "45°-wire") are handicapped with this error. It has been part of the general expended efforts since 1940, to make the wind tunnels as turbulence-free as possible, in order to get exactly uniform results for tests at different wind tunnels on identical airfoils, at identical Re-numbers; in that sense it is appropriate to provide model support that is as free as possible of outside influences. Model flight practice asks basically for two flight performance characteristics:

1. The model should reach a good distance, should glide the longest possible distance for the available glide altitude H, i.e., have a good glide ratio.

   $$\varepsilon = \frac{H}{B} = \frac{W}{A} = \frac{c_w}{c_a} = \frac{c_y}{c_x} = \tan q.$$

   Glider models reach about 1:18 = 0.056 as the best glide ratio, high performance type gliders 1:40 = 0.025. To obtain integral numbers instead of the inconvenient fractions one uses the reciprocal of the glide ratio c_a/c_w, which is designated as glide coefficient. In the polar diagram Fig. 16 the tangential polar line results in the optimum glide coefficient of the specific profile and the specific aspect ratio.

2. More important than the glide distance for the model flight is the smallest possible rate of descent v_y, which has a minimum for each airfoil at an angle of attack approximately 1 to 2° larger than the one belonging to (c_a/c_w) max, i.e., at that value α where the lift coefficient (c_a^3/c_w^2) reaches a maximum. The rate of sink

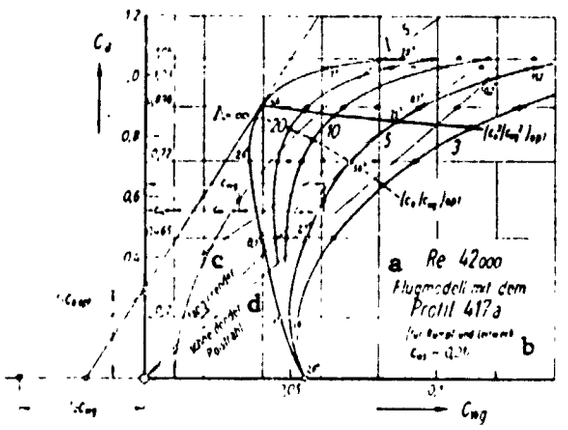

Fig. 16. Polar diagram for flight models with profile 417a for eight different airfoil aspect ratios. Approximate determination of optimum lift coefficients c_a^3/c_{wg}^2 according to Klemper. Approximate determination of optimum glide values c_a/c_w through the tangential polar line.

Key: a - Flight model with
b - (for fuselage and tail assembly)
c - tangential
d - sectioning polar ray

$$v_y = \sqrt{\frac{G}{F}\frac{2}{\rho}\frac{1}{c_a^3/c_w^2}} \text{ [m/s]}$$

is only dependent on this lift coefficient, in addition to the wing load G/F and air density ρ. For approximate determination of values c_a, c_w and α belonging to $(c_a^3/c_w^2)\max$, the design drawn in Fig. 16 according to Klemperer is sufficient.

An absolute comparison is given only by the airfoil drag $c_{w\infty}$ converted for the infinite aspect ratio, or by the airfoil glide coefficient $c_a/c_{w\infty}$ and by the lift coefficient $c_a^3/c_{w\infty}^2$. For the previously discussed airfoils N60, 417a and 417b--with and without turbulator--the curve of the airfoil lift coefficient for five different Re-numbers is plotted in Fig. 17, by adding the values for the flat plate and for the 9%

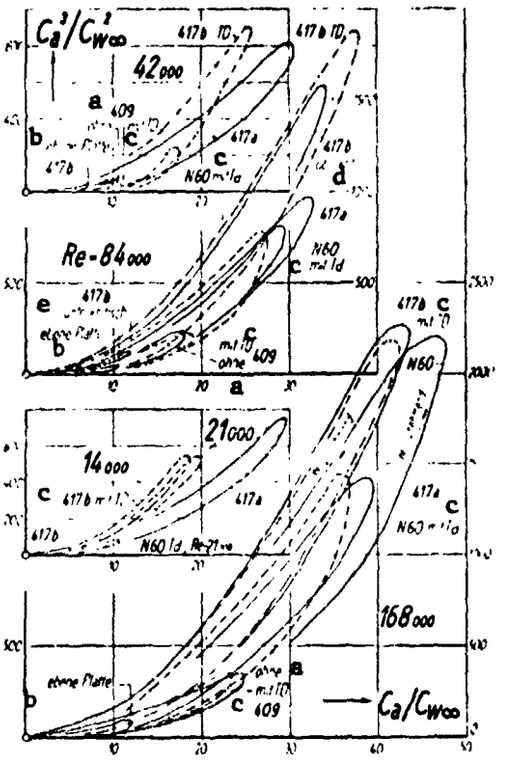

Fig. 17. The comparison of profile lift coefficients and profile glide coefficients (in 5 different Re-number steps) makes possible the clearest evaluation of the airfoil profile performance as a function of the Re-number. TD means testing in the turbulent wake of a wire of 4 m/m dia, Td means that a turbulence wire of 0.7 m/m dia is fastened to the model.

Key: a - without
b - flat plate
c - with
d - hypercritical
e - subcritical

thick symmetrical profile 409. Since the cube of c_a appears in the lift coefficient, this efficiency comparison highlights the optimum values for pure airfoils clearly.

Re = 14,000 and 21,000. At 14,000 only measurements for airfoil 417b are available. With Td 417b is by far better than without it. It is surprising, however, that it is not more effective at 21,000 and that it is far surpassed by 417a, which could already be gathered from Fig. 15.

Re = 42,000. The turbulence effect is particularly effective for airfoil 417b. But even here its lift coefficient is inferior to airfoil 417a.

Re = 84,000. Here the difference between 417b with and without Td is only small, both are superior to all others in the region of 63,000 to 100,000. If, during a lull or gust, the airflow separates for

"airfoil 417b without turbulence string," then the lift and glide coefficients drop severely, which does not occur with a turbulence string. This clearly explains that for comparison flights with a turbulence string the practically documented improvement of starts and flight qualities (especially gust stability) is valid. In contrast to this /1 the flat plate and the symmetrical airfoil profile 409 are bad lift producers. Profile 409 works even in turbulent airflow only marginally better.

Re = 168,000. As already visible from Fig. 15, the airfoil N60 without turbulator is greatly superior to the same airfoil with Td, as well as to airfoil 417a. It is surprising, however, that the heavily cambered plate 417b, with and without Td, is only slightly inferior to airfoil N60. At this comparatively high Re-number for model flight the 12% thick airfoil N60 is preferable due to its greater stability and smaller motion of the stagnation point.

12. Airfoil profile selection according to Re-numbers. The airfoil selection is made according to the diagrams[1)] in such a manner, that a blower vane or a model airfoil should safely work hypercritically and that a sufficiently great hypercritical Re-number region remains up to the subcritical flow separation. In the Re-region <200,000 the following is generally valid:

1. The thicker a profile, the higher is the Re-number at which the transition to turbulence occurs, or: the smaller the

---

[1)] For profile selection and technical application test results are shown in 28 numerical tables and 20 diagrams for the Re range 21,000-168,000, on 5 airfoil profiles (which illustrate the problem through extreme contrasts in the initially mentioned book [18]. The tests give exact information from which Re-number on it is beneficial to shape a blower vane.

Re-number of the flight model or of the blower vane, the thinner the profile must be and the smaller the nose radius.

2. Only in the subcritical region and within the transition zone does artificial turbulence improve the effectiveness of the profile, since the start of the transition is moved towards the lower Re-numbers.

3. While thin, slightly cambered plates (f < 6.5%, r < 1%) work better without turbulators, turbulence generation produces remarkable improvement for larger cambered airfoils.

4. At Re = 150,000 even the heavy profiles work hypercritically so that it presents the limits of the turbulence effect for them as well while for standard profiles, of medium thickness and camber, Re is about 100,000.

5. Symmetrical profiles are bad lift generators, with or without turbulator (as is the flat plate). Thick symmetrical profiles are only advantageous at very high Re-numbers.

13. Comparison: Large aircraft and flight model. From airfoil tests at low Re-numbers the following surprising contrasts are obtained:

1. While on a large airplane the airflow around the wings is always hypercritical, since the boundary layer becomes turbulent after a laminar start, for airflow around the model airfoil a bad subcritical flight condition is possible because of a stable laminarity of the boundary layer in the Re-number range <100,000.

2. For the large airplane it is desirable that the boundary layer remain laminar as long as possible to utilize the

smaller laminar friction as far as possible and to delay the turbulent separation due to turbulent friction loss up to the largest possible angle of attack; for the airplane model, however, the earliest possible turbulence is desirable to attain a large hypercritical Re-number range.

3. For the large glider one selects, therefore, a round-nosed, thick airfoil and for the small flight model a sharp-nosed, thin airfoil. For the high speed aircraft one chooses a laminar profile with very little camber of the profile center line, but large rearward position on the location of greatest profile thickness, for the flight model a turbulence profile with great camber at the profile center line and small camber at the rearward position.

4. The aircraft wing should be as smooth as possible for low surface friction, especially at the leading edge. At the leading edge of the flight model a certain roughness and even a tripping edge may be advantageous. For the flight model the surface friction is of lesser importance.

5. All means of artificial turbulence, like surface roughness, a sharp leading edge, a tripping edge at the profile nose and especially turbulence strings in front of the leading edge, are favorable for the flight model below the hypercritical fully turbulent Re-number range; they are always unfavorable for large aircraft.

6. For the large aircraft the elliptically sweptback circumference of the wing and the propeller is advantageous for production of low induced drag; for the flight model and the propeller of the flight model the more rectangular circumference at equal aspect ratio is more likely to obtain as hypercritical an Re-number range as possible, resp. to

avoid subcritical operation of the wing tips. For a twisted rectangular wing of the flight model elliptic lift distribution may also be obtained.

7. While present gliders achieve a glide coefficient of 25 to 40, glider models only reach coefficients of 10 to 18 hypercritically, corresponding to the lower Re-number.

14. Examples of Application.

Glider models: the Federation Aeronautique Internationale (FAI) has prescribed a minimum surface loading of 12 g/dm^2 for model flight in the presently valid contest directives, the wing area is understood to be the vertical projection of the wing and the elevator control surface. The inclusion of the elevators is justified since for flight models, in contrast to large aircraft, they are mostly set up to complement the lift. For the A 2-class a total area of 32 to 34 dm^2 and 410 g total weight is specified. To facilitate the practical application of the airfoil measurements for the model flyer, Fig. 18 presents the construction data for the profile test N60 for 14 glider model sizes in the hypercritical region for Re = 84,000 and 105,000 and 7 different aspect ratios, for which the wing with a wing load of 12 g/dm^2 obtains the lowest sink rate, i.e., flies with optimum lift. The detrimental drag of fuselage plus control surfaces is considered through C_{ws} = 0.01. For each model 9 sizes are presented. Intermediate values may be extrapolated. /163

Since the choice of size and load of the controls is arbitrary that must be taken into consideration through reduction of the test data by calculation. Velocities v_x and v_y change as the square root of the ratio of partial surface load of the wing to the required total load of 1.2 Kg/m^2. From Fig. 19 the variable data for "Model Re = 105,000 and A = 10" may be obtained for the various control surface sizes and loads.

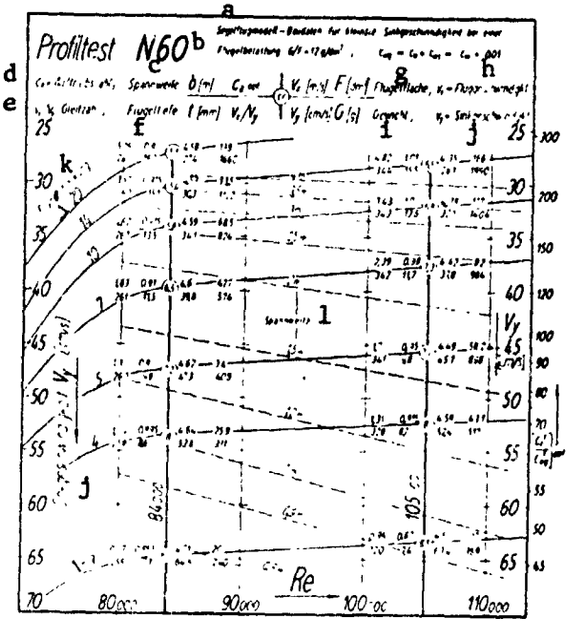

Fig. 18. The "profile test N60" provides the data construction of glider models with the lowest sink rates when using profile N60 and surface loading of 12 g/dm².

Key: a - Glider model -- design data for minimum gliding velocity
b - wing stress
c - wing spread
d - lift coefficient
e - glide ratio
f - wing depth
g - wing area
h - flight velocity
i - weight
j - sink rate
k - aspect ratio
l - wing span

Bird flight: Since the flight model, because of its size and its Re-number, is more similar to birds than large aircraft, several interesting correlations found in the study of bird flight may be expected for the model flight. One can observe various applications of the turbulence effect in the flight of birds. For instance, the single file gliding flight of vultures may be explained in that way, that the vulture in the lead is the turbulence generator for those that follow. In the v-formation flight of migrating birds the turbulence of the wing boundary layer of the bird behind him plays a role during wingflapping flight besides the utilization of the rising edge eddies and the aerial billow (air wave) of the bird flying immediately ahead. Utilization of the two least mentioned effects is also valid for the formation flight of ducks. Moreover, the wedge formation in the flight of birds and insects -- besides utilizing local thermals -- may be interpreted as turbulence effect. As result of the wind tunnel test on the plaster cast model of a seagull a critical transition at Re = 105,000, with a glide coefficient improvement from 7.5 to 12.5, was measured [9].

An interesting possibility for airfoil profile configuration for the gain of great spar depths is indicated by the wing cross-section of the vulture which is known as an excellent glider. The vulture wing profile has a tripping edge on the bottom side behind a steeply cambered, thin, leading edge, which localizes the transition vortex and maintains turbulence of the bottom side flow even at large angles of attack. This edge has also been identified on storks, cranes, kites and flamingos. Behind this tripping edge are the upper or lower arm bones, respectively, and the thick extensor muscle. The tripping edge recedes the most at the elbow. The flexor muscle, which is particularly thin for landgliders is found in the wing's leading edge. Upper arm, lower arm and flexor muscle form a triangle, which is covered by the frontal section of wing skin. During comparable observations of the gliding flight of birds Hankin [10] established that vultures and kites, whose tripping edge at the wing bottom side is particularly sharp, circle faster and ascend faster than eagles in spite of higher wing surface loading. Idrac [11] could measure a minimum sink rate of 0.42 m/s for kites at a glide velocity of 7 m/s, which corresponds to a glide coefficient of 17.

The wing load for birds varies between 16 kg/m^2 for the albatross to 1.7 kg/m^2 for the swallow, to that of the butterflies from 0.17 to 0.1 kg/m^2 (1 g/dm^2). Following the aerodynamically related example from nature, the wing load of flight models is in the same range with 4 to 0.1 kg/m^2, where the lower limit corresponds to hangar flight models covered with microfilm. The wing load of gliders amounts to from 20 to 10 kg/m^2, which is 5 to 200 times as great. Using light construction, particularly through the use of Balsa wood, (γ = 0.15 to 0.25) the model achieves an equal or smaller sinking rate in spite of an aerodynamically limited, bad glide coefficient. Present glider models achieve a minimum sink rate of about 0.25 m/s in still air.

In Fig. 20 some examples are shown of means for generation of the /164
high lift of bird wings, which are also known to airplane technology [12]. The soaring wring (a) of the land gliders (vulture, kite, stork, buzzard) has an almost rectangular contour for outspread flapping wings, which generate lift as well as forward motion according

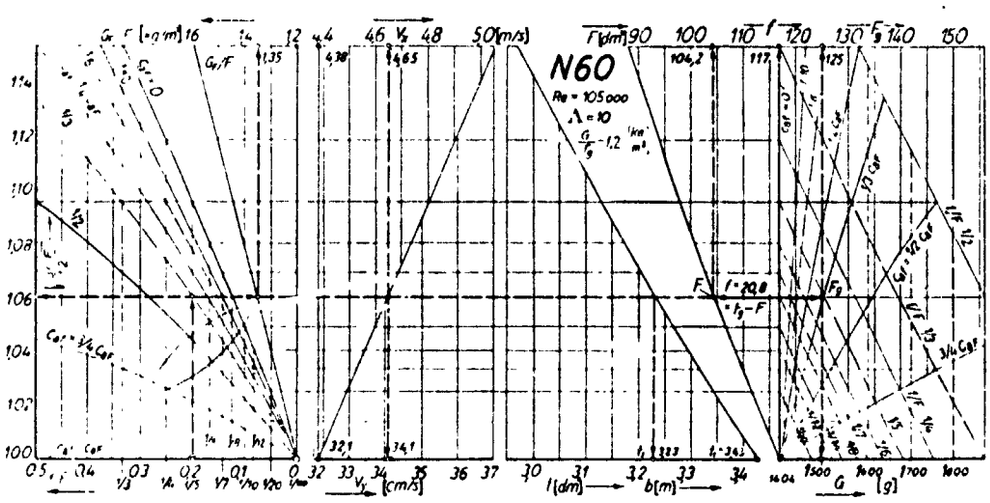

Fig. 19. Supplementary diagram for profile test N60 for models with an aspect ratio of A = 10 in consideration of various sizes and loads of elevator controls. F = wing area, f = control area, F_g = f + F; G = flying weight. Illustrated example: f/F = 1/5; c_{af}/c_{aF} = 1/3.

to the angle of attack. The land gliders soar mostly in static sailing flight in regions of thermal updrafts in front of mountain slopes, in the leeward waves of the air current, etc. For dynamic soaring the extended jointed wings of the seagoing gliders are especially suitable, as for instance the albatross and the seagull (c), since their wings are easily rotated as integral unit to take advantage of variations of the wind. The lifting of the cover feathers of the seagull from its flapping wings (c) results in a large uplift during landing (landing flaps) and the split flap produces large drag as an air brake. Moreover, the fixed position vortex cone vanishes without hysteresis when the seagull continues on from this condition. The outspread tail of the forked tail falcon corresponds to the aileron patent by Junkers.

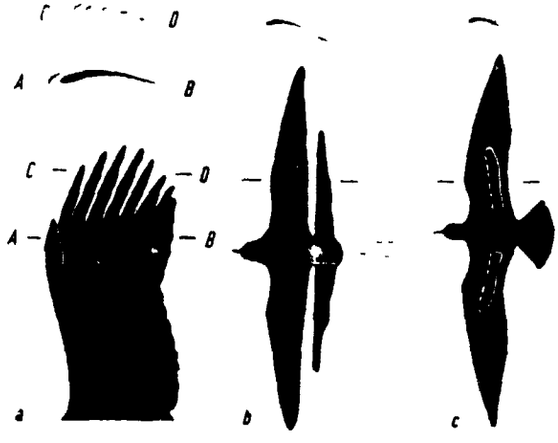

Fig. 20 High lift devices on the wings of birds : a) Landglider ; thumb feathers as slats ,widespread finger feathers as slotted wing; b) Forked-tail falcon with widespread tail serving as aileron ; c) Seagull during landing with cover feathers raised to act as slat and limiter of flow separation.

The biologist E. v. Holst [13] succeeded in interpreting the problems of control surfaces in the flight of large birds, elucidating them by means of aerodynamic measurements and by designing ornithopter models using interesting transmissions. The schematic Figure 21 [14] presents the reciprocal varied adaptation of the angle of attack for the large wingtip feathers and main (arm) wing flaps to the sinusoidal motion of the wing. At the down stroke of the wing, which is performed with great force, the wing tip generates lift H_1 and the strong

forward thrust S, while the main wing moves along passively. At the upstroke the main wing, which glides along a flatter wave trajectory, generates lift H_2 which is, however, subject to a small negative thrust R, with the wingtip now moving along passively. Only in this manner does the bird succeed in maintaining a straight line flight trajectory. Without the lift performance of the main wing at the up stroke the bird's center of gravity would move up and down with the rhythm of the wing strokes.

This model of an ornithopter confirms, through the naturalness of its flight qualities and good flight performances, the validity of this insight. According to E. v. Holt, nature has employed ornithopter flight on four occasions with different biological materials and at different times: (1) insects; (2) with the flying dinosaurs; (3) with birds; and (4) with bats [15].

15. Aeronautical areas of application.

The first known flight of a flight model by the Englishman Stringfellow which,driven by a steam engine and two opposing pusher propellers and built according to the prototype by Henson, succeeded in 1848 and is considered as the birth of modern aeronautics. Save for the flight-mechanical data gained by Pinaud, Lilienthal, Lanley, Lanchester, Ahlborn, etc., only few quantitative fundamentals could be gained from tests on free flight models. The wind tunnel displaced the free flight model as research apparatus, since it is by far simpler to blow air against a 1:10 scale model of an aircraft with 10 times the velocity to attain the Re-numbers of the large aircraft. /165
Where airfoil tests in the wind tunnel are available for low Re-numbers as well as for high Re-numbers, broader conclusions may be drawn from flight tests on free flight models,which can be especially important for flight trials of novel configurations as an inexpensive preliminary test.

When flight tests are performed in a large wind tunnel then disturbing influences of wind, temperature and turbulence are to be

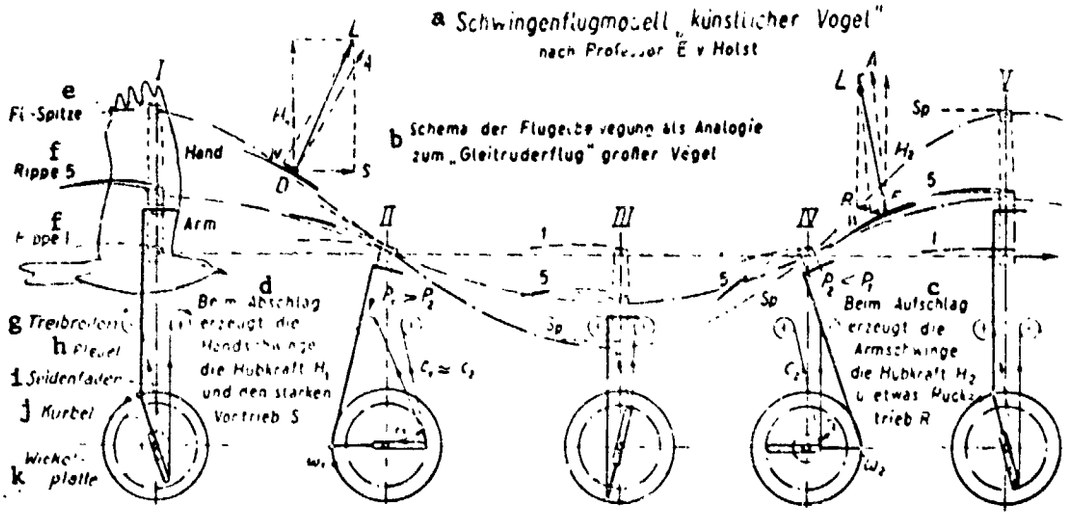

Fig. 21. Schema of wing motion and components of the aerodynamic force of an ornithopter model with connecting rod drive (after E. v. Holst).

Key: a - Ornithopter model "artificial bird"
b - schematic of wing motion as analogy of "glide rudder flight"of big birds
c - at landing the arm flap generates the lift force H_2 and same repelling force R
d - at takeoff the hand flap generates the lift force H_1 and the strong thrust S
e - wing tip
f - Rib
g - drive rollers
h - connecting rod
i - silk strings
j - crank
k - coiling plate

avoided. For measurement of nonaccelerated glider flight simple means are sufficient: a stopwatch, tape measure, surveyor's rod for sighting the altitude of the flight. Flight trajectory angle and angle of attack of the airfoil can also be obtained from photographs in front of vertical lines. The glider tests become more accurate when a suitable catapult provides adequate velocity and gliding position for the model. Starting of aircraft models by means of an elastic launching rope of 10-100 m length in still air, resp., at a temperature inversion, permits longer test flights during which rotary motion is measured according to the method mentioned by Raethjen [16] with a range finder or cinetheodolite, or from the glider according to Raspet's [17] method for observation of bird flight.

For interpretation and evaluation of model tests in the inclinable free-flight wind tunnel and in a spinning wind tunnel, available

available and additional wind tunnel measurements in the region of low Re-numbers on airfoils, fuselages, etc., are indispensable for correct understanding of the subcritical detailed processes and to avoid them by providing means for local turbulence. It should also not be too difficult to let a free flight wind tunnel operate as closed pressure chamber by means of compressed air so as to achieve a considerable increase in the Re-number and so obtain a hypercritical condition for small model parts.

The air flow around individual components can be subcritical at low flight not only in model tests but also for the actual aircraft, e.g., on profile struts, instrument supports and such, on gliders and rotary wing aircraft. This is valid especially for flight at great heights, since Re at 11 Km altitude is reduced to 1/2.6 and at 20 km to 1/8.5. The subcritical condition may thus occur at the loss of velocity, not only for the components mentioned but also on extremely pointed control surfaces, e.g., propellers and on compression vanes of motors and turbines. For the same reason a strong tapering off of the wing tips should be avoided in high flying gliders.

Tests with manned model airplanes should also be mentioned here; they are built as scaled down models of projected large aircraft under consideration of the laws of similarity. Test flights that are too dangerous for a manned aircraft, are executed by smaller, electronically remote controlled jet models, as reported recently from the U.S.A.. Such models, which were developed through long-term research projects, weigh no more than can be carried by one man. To change the trimming by weights, the ballast and accessories inside the model are adjustable. These tests made possible the shortening of the previously required development time by a considerable amount and enormous lowering of the development costs, especially by elimination of tests in the giant wind tunnel.

In addition to the already well known military applications there will certainly be some peacetime applications for electronically remote controlled models. Especially promising is their application for

research of updrafts at locations for glider flight. Equipped with radio transmitters such models may also hold promise as apparatus for meterological research.

The foregoing explanations qualify the necessity for sponsorship of model aeronautics, including small combustion engines, electronic model equipment and particularly the aerodynamics of low Reynolds-numbers, which is required as a fundamental consideration.

REFERENCES

1. L. Prandtl and A. Betz: Ergebnisse der Aerodynamischen Versuchsanstalt zu Göttingen [Results from the Aerodynamic Research Center at Göttingen]. Publishers: R. Oldenbourg, Munich, issues I to IV

2. L. Prandtl and O. Tietjens: Hydro- und Aerodynamik Band 1 und 2 [Hydro- and Aerodynamic, Volume 1 & 2]. Publishers: Springer, Berlin, 1929.

3. H. Schlichting: Grenzschicht-Theorie [Boundary Layer Theory]. Publishers: G. Braun, Karlsruhe, 1950.

4. S. Hoerner: Versuche mit Kugeln betreffend Kennzahl, Turbulenz und Oberflächenbeschaffenheit [Tests with Spheres Relative to Index, Turbulence, and Surface Condition]. Luftfahrtforschung (Aeronautics Research), 1935.

5. R. C. Platt: Turbulence factors of NACA wind tunnels as determined by sphere tests. NACA Ref. 558 (1936).

6. H. Schlichting. Die Entwicklung der Windkanäle in den letzten Jahrzehnten [The development of wind tunnels in recent decades]. Almanac 1952 of WGL. Publishers: E. Vieweg & Son, Braunschweig, 1953.

7. R. Seifert: Messung der Kanalturbulenz mittels Kugel und ihr Zusammenhang mit der Hitzdrahtmessung [Measurements of wind tunnel turbulence with a sphere and its connection with hot-wire measurements]. Monograph D, 4.2. of AVA Gottingen.

8. F. W. Lanchester: Aerodynamik [Aerodynamics]. Publisher: Teubuer, Leipsie, 1909.

9. F. Feldmann: Windkanaluntersuchung am Modell einer Möve [Wind tunnel test on the model of a seagull]. Aero-Revue, July 1944.

10. Th. Dreisch: Der Segelflug der Vögel [The glider flight of birds]. Reports and Proceedings of the WGL, Bulletin 9, 1922.

11. P. Idrac. Experimentelle Untersuchungen über den Segelflug der Vögel [Experimental research of the glider flight of birds]. Translated by F. Hohndorf. Publisher R. Oldenbourg, Munich, 1932.

12. D. Kuchemann and E. v. Holst: Zur Aerodynamik des Tierflugs [On the aerodynamic of animal flight]. Luftwissen No. 9, 1942.

13. E. v. Holst: Über „künstliche Vögel" als Mittel zum Studium des Vogelflugs [On "artifical birds" as means for the study of bird flight]. Journal for Ornithology 91 (1943).

14. F. W. Schmitz: Das Schwingenflugproblem nach E. v. Holst [The ornithopter problem according to E. v. Holst]. Construction plan for an ornithopter flight model with building instructions, 1954.

15. E. v. Holst: Tierflug und Menschenflug [Animal flight and human flight]. Physics papers [Physikalische Blatter) Vol. 7, Bulletin 12.

16. P. Raethjen: Flugmessungen [Flight measurements]. Zeitschrift für Flugtechnik und Motorluftschiffahrt 1925 S. 235, 1926 S. 537, 1929 S. 413.

17. A. Raspet: Leistungsmessungen an einem Segelvogel [Performance measurements for a soaring bird]. Thermik, Bulletin 10, 1951.

18. F. W. Schmitz: Aerodynamik des Flugmodells [Aerodynamics of flight models]. 2nd edition, Carl Lange Publishers, Duisburg, 1952.